Hindawi
Wireless Communications and Mobile Computing
Volume 2022, Article ID 5850187, 9 pages
https://doi.org/10.1155/2022/5850187

Research Article

Damage Detection Test of GFRP Composite Civil Materials Based on Piezoelectric Ceramic Sensors

Yanhua She and Gaojie Cai

School of Urban Construction, Yangtze University, Jingzhou, 434023 Hubei, China

Correspondence should be addressed to Yanhua She; syh916@126.com

Received 15 July 2022; Accepted 22 August 2022; Published 10 September 2022

Academic Editor: Chia-Huei Wu

The piezoelectric ceramic sensor was fixed on Glass Fiber Reinforced Plastic (GFRP) composite civil materials, using the external paste method for damage detection test. The effect of the depth and number of cracks on the surface of the GFRP specimen on the signal received by the piezoelectric ceramic sensor was studied. The time-domain signal graph and energy graph based on wavelet packet were drawn, combining the active induction method and the energy method based on wavelet packet. It is found that the greater the damage degree of GFRP specimens, the smaller the voltage value of the signal, the smaller the energy of the signal, and the greater the damage index based on wavelet packet. The results showed that the active induction method can be used to collect the data of GFRP specimens by piezoelectric ceramic sensor. The collected data are processed by using the damage index principle based on wavelet packet. The maximum voltage value of the specimen, the energy of wavelet packet, and the damage index based on wavelet packet can all accurately judge the damage change of GFRP specimens. The active induction method based on piezoelectric ceramic sensor can detect the damage change of GFRP specimens in real time. It provides an effective method for damage analysis of GFRP composite civil materials.

1. Introduction

In recent years, the technology of civil engineering structural damage detection [1–4] and health monitoring [5–11] has developed rapidly. In particular, based on the active induction method of piezoelectric effect, the identification and diagnosis of structural damage can be realized by analyzing the difference between the original signal and the current signal [12–21]. Piezoelectric ceramic sensors based on lead zirconate titanate (PZT) have many advantages, such as rapid response, strong energy collection ability, low cost, and easy implementation [22–26]. Roh [27] proposed an active induction monitoring technology, which embeds multiple piezoelectric patches into the composite structure to detect the damage of the composite plate. Subsequently, the technology is widely used in damage detection and structural health monitoring in civil. Du and Kong [28, 29] damaged the pipeline by corrosion and cutting and used piezoelectric ceramic sensors to detect pipelines with different damage levels, to study the change of stress wave after pipeline damage. Feng et al. [30] used piezoelectric ceramic sensors to detect the damage of concrete and found that this method was feasible for detecting cracks in concrete. Zhang et al. [31] took the initiative to cut the wood, resulting in varying degrees of damage. Piezoelectric ceramic sensors were used to detect the changes of stress waves before and after wood damage. Huo et al. and Wang and Hou [32, 33] used piezoelectric ceramic sensors to detect bolt loosening. Yin et al. [34] optimized the active induction method and used piezoelectric ceramic sensors to detect bolt loosening in a washing machine. Song et al. [35] used piezoelectric ceramic sensors to monitor the bolt of rock reinforcement components to ensure that the bolt can play an important role in the normal operation of underground mines. Xu et al. [36] used a homemade piezoelectric ceramic sensor to detect the concrete and found that the strength of the concrete is related to the voltage value obtained by the detection. Feng and Xiao [37] proposed a passive sensing method based on piezoelectric ceramics to detect typical damage types of concrete piles, including partial mud invasion,

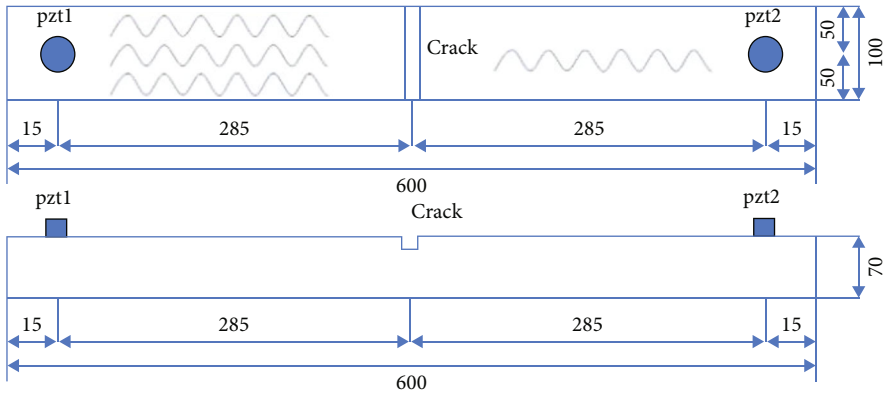

Figure 1: Active induction method (unit: mm).

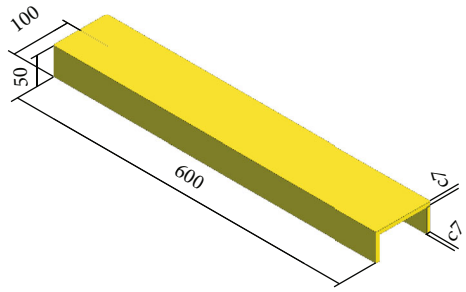

Figure 2: Schematic diagram of GFRP specimen (unit: mm).

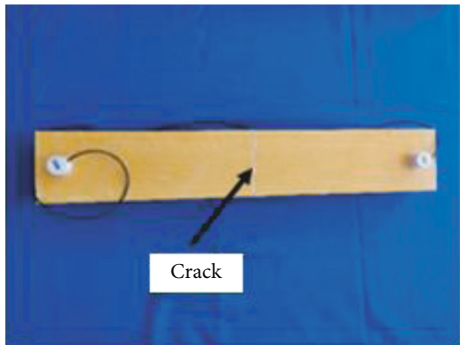

Figure 3: The specimen with damage.

Figure 4: Piezoelectric ceramic sensors.

secondary concrete pouring interface, circumferential cracks, and all mud invasions. Liu et al. [38] buried piezoelectric ceramic sensors in reinforced concrete and used the impedance method to detect the corrosion of steel bars. The results showed that after the annular piezoceramic disk was encapsulated, the resonance of the piezoelectric ceramic under the effects of electric excitation was restricted due to the damping effect of the packaging layer. Kong et al. [39, 40] used piezoelectric ceramic sensors to study soil water content. The experimental results showed that the received signal energy has a certain correlation with soil water content. Rao et al. [41] proposed a new ultrasonic guided wave tomography (GWT) system based on a self-designed piezoelectric sensor for online corrosion monitoring of large plate-like structures. Qin et al. [42] combined the piezoelectric ceramic sensor with the active induction method to detect the bond-slip between steel plate and concrete. However, there are few studies on damage monitoring of Glass Fiber Reinforced Plastic (GFRP) by the active induction method using piezoelectric ceramic sensors.

GFRP is a new type of civil composite material based on resin and filled with glass fiber. It has the advantages of light weight, high strength, heat resistance, corrosion resistance, good insulation, low production energy consumption, and environmental protection [43]. Therefore, it is widely used in the field of civil engineering and construction, but GFRP damage detection is rarely done. In order to analyze the damage of GFRP specimens more accurately and effectively, this paper combined the active induction method with the energy based on wavelet packet. On the basis of analyzing the maximum voltage value, the signal energy was further analyzed. The time-domain signal diagram and the energy diagram based on wavelet packet were obtained.

2. Detection Principle

2.1. Active Induction Method. In this experiment, the active induction method was used to detect the damage changes in GFRP specimens by piezoelectric ceramic sensors. The sensor PZT1 generates the stress wave, which will propagate in the whole specimen and be received by another sensor PZT2. When cracks or holes occur in the specimen, the stress wave will reflect the wave generated by the defect,

Table 1: Main performance parameters of piezoelectric ceramic sensors.

Density ($g \cdot cm^{-3}$)	Dielectric constant ε	Electromechanical coupling coefficient	Capacitance C (nF)	Curie temperature T_c (°C)	Mechanical quality factor Q_m
7.5	1600	1.65	3.77	300	80

Table 2: Test conditions.

	Specimen number	Number of crack n	Crack depth h (mm)
Group A (GP-A-n-h)	GP-A-0-0	0	0
	GP-A-1-1	1	1
	GP-A-1-3	1	3
	GP-A-1-5	1	5
	GP-A-1-7	1	7
Group B (GP-B-n-h)	GP-B-0-0	0	0
	GP-B-1-3	1	3
	GP-B-3-3	3	3
	GP-B-5-3	5	3

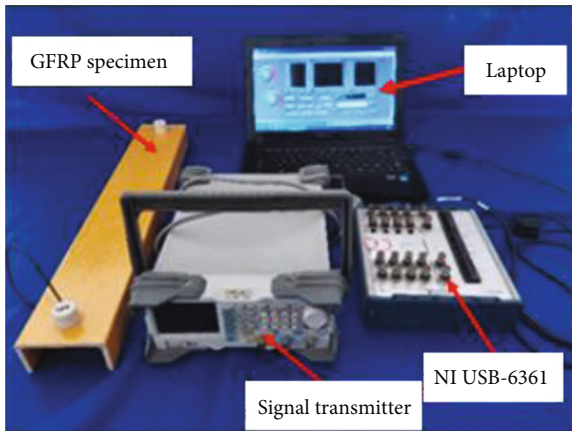

Figure 5: Test device.

resulting in a decrease in the signal received by the sensor PZT2. The deeper the defect, the less signal the sensor PZT2 receives, as shown in Figure 1. In order to quantify the damage of GFRP specimens, the energy method based on wavelet packet is used.

2.2. Energy Method Based on Wavelet Packet. The wavelet packet analysis can effectively decompose various time-frequency signals [12]. The energy method based on wavelet packet is usually used to calculate the energy of the received signal in structural analysis. In this study, the energy analysis based on wavelet packet was used to calculate the received wave signal energy under different damage levels in GFRP specimens. The calculation steps are as follows:

Firstly, the original signal S received by the sensor is decomposed into 2^n signal subsets with different frequency bands by n-level wavelet packet decomposition. Signal subset X_j, where j is the frequency band ($j = 1, 2, \cdots, 2^n$) and can be expressed as

$$X_j = \left[X_{j,1}, X_{j,2}, \cdots, X_{j,m}\right], \tag{1}$$

where m is the data sampling of the decomposed signal subset.

Secondly, the energy of signal subset $E_{i,j}$ can be defined as

$$E_{i,j} = \left[X_{j,1}^2 + X_{j,2}^2 + \cdots + X_{j,m}^2\right], \tag{2}$$

where i is the ith measurement value. The signal energy of the ith measurement can be expressed as

$$E_i = \left[E_{i,1}, E_{i,2}, \cdots, E_{i,2n}\right]. \tag{3}$$

Thirdly, the received signal energy can be calculated as

$$E = \sum_{i=1}^{2^n} E_{i,j}. \tag{4}$$

In this paper, based on the wavelet packet energy method, the received wave energy of GFRP specimens under different damage conditions will be calculated.

In the fourth step, the damage index of the structure (DI) is

$$\mathrm{DI} = \sqrt{\frac{\sum_{j=1}^{2^n}\left(E_{i,j} - E_{h,j}\right)^2}{\sum_{j=1}^{2^n}\left(E_{h,j}\right)^2}}, \tag{5}$$

where $E_{h,j}$ is the energy of the j signal of the last layer decomposed by the wavelet packet in the healthy state of the structure. The greater the damage index (DI), the higher the attenuation of the stress wave in the propagation process, and the larger the degree of structural damage.

When the damage index (DI) is 0, the specimen is not damaged, and when DI is 1, the specimen is completely destroyed. However, the damage index can only evaluate the damage change of a single specimen, and the damage between multiple specimens cannot be compared. The reasons are as follows: first, the piezoelectric ceramic sensor is highly sensitive and is easily affected by the environment such as temperature and noise, second, the coupling agent between the sensor and the specimen will affect the collected data, third, the parameters of the signal transmitter will affect the signal energy, and fourth, the difference of the sensor itself will have an impact on the received signal.

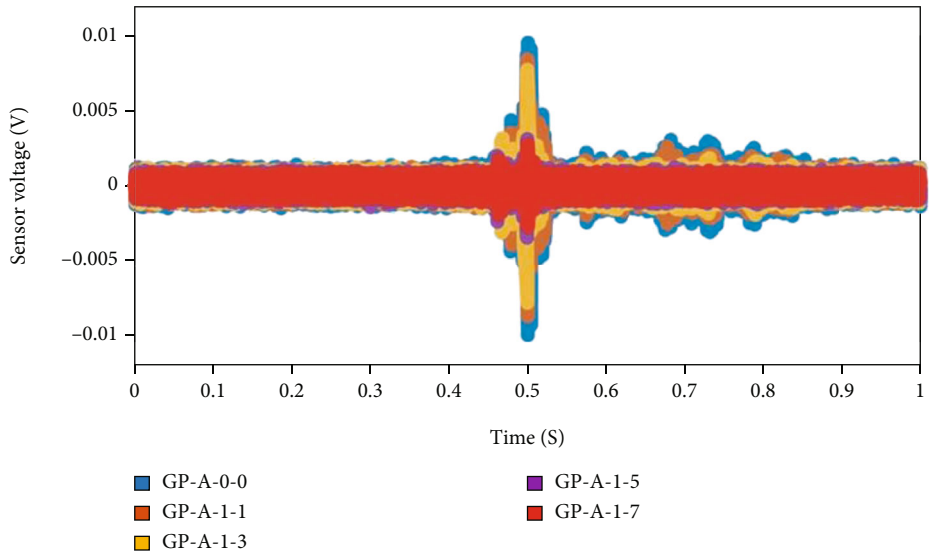

Figure 6: Time domain signal diagram of group A specimens.

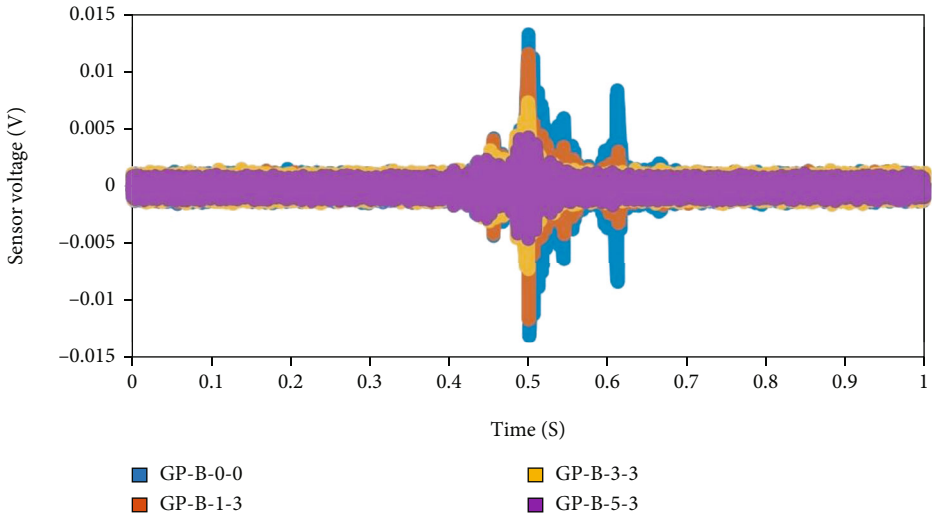

Figure 7: Time domain signal diagram of group B specimens.

3. Test Overview

3.1. Specimen Design. According to the different manufacturing process, GFRP produces two different types. The first is the pultrusion type, which has very strong tensile strength, but slightly insufficient compressive strength. The second is the winding type, which is opposite to the former. It has very strong compressive strength and weak tensile strength.

In this test, nine GFRP specimens with the same size and different damage degree were designed by using the pultrusion type. As shown in Figure 2, the size of each specimen is 600 mm in length, 100 mm in width, 50 mm in height, and 7 mm in wall thickness. As shown in Figure 3, two piezoelectric ceramic sensors were fixed on the surface of each specimen by the external sticking method, and the fixed coupling agent was epoxy resin, which was the connection interface between the piezoelectric ceramic sensor and GFRP. As shown in Figure 4, the sensor PZT-5H is selected in the test. The size of the sensor is 15 mm in diameter and 20 mm in thickness. The piezoelectric ceramic sheet is wrapped by two cylindrical marbles. The marbles protect the piezoelectric ceramic sheet and prevent the violent collision of the outside world. The main parameters of the piezoelectric ceramic sensor are shown in Table 1. There are nine specimens in this test, which are divided into group A with five specimens and group B with four specimens. As shown in Table 2, in group A, the number of crack is 1, and the crack depth is 0, 1, 3, 5, and 7 mm, respectively. In group B, the crack depth is 3 mm, and the number of crack is 0, 1, 3, and 5, respectively. For example, GP-A-1-3 indicates that the number of cracks in Group A is 1 and the depth of cracks is 3 mm. For all test specimens, the crack width is set to 1.5 mm.

3.2. Test Equipment. As shown in Figure 5, the test device consists of a data collector (NI USB-6361), a signal transmitter, a laptop, and the GFRP specimens. The sampling

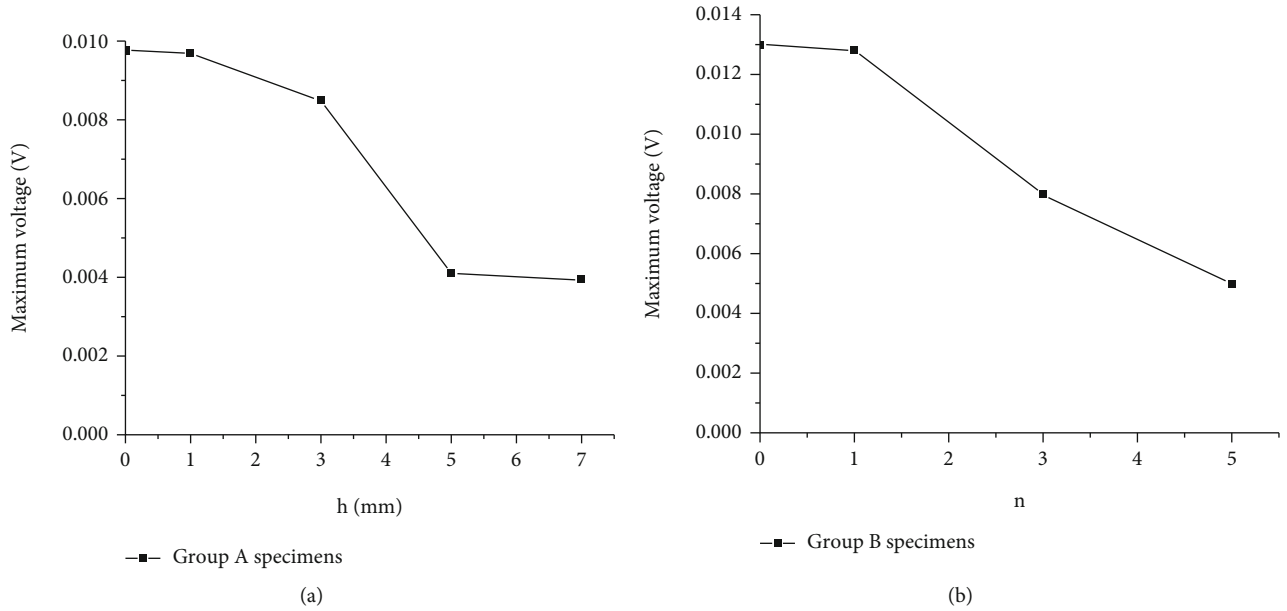

Figure 8: Maximum voltage value of GFRP specimens. (a) Group A specimens. (b) Group B specimens.

frequency of the data acquisition system is 2 MS/s. This parameter means that the data collector can collect 2 million valid data within 1 second. When the stress wave propagates in the material at a certain frequency, the energy of the stress wave will decrease during the propagation process. The frequency of the stress wave affects the propagation of the stress wave in the material. The proper frequency will make the stress wave travel farther, and the signal received by the sensor will be more stable. Signal transmitter adopts the frequency sweep mode, that is, within a cycle, the frequency changes from the start frequency to the stop frequency. A fixed frequency often leads to instability of the signal, so a fixed frequency is not selected. In order to ensure the normal operation of piezoelectric ceramic sensors, appropriate voltage should be set. If the received signal is weak in the test, it is necessary to debug the start frequency and stop frequency of the signal transmitter. The start frequency, stop frequency, voltage value, and period of group A specimens are 10 Hz, 100 kHz, 10 V, and 1 s, respectively. Multiple cracks were cut out on group B specimens, resulting in excessive energy loss. The signal strength received by the sensor of group B was weak. In order to carry out the test smoothly, the frequency was increased to improve the signal strength received by the sensor. Therefore, the start frequency, stop frequency, voltage value, and period of the test pieces in group B are 100 Hz, 500 kHz, 10 V, and 1 s, respectively. To minimize the impact of the environment on the results, all tests were performed in a closed and quiet laboratory.

3.3. Test Process. The piezoelectric ceramic sensors used in this experiment are very susceptible to external temperature and vibration. Therefore, it is necessary to make strict requirements on the environment during the test. Before the formal test, all test-related items should be placed in a closed laboratory for 2 to 3 hours to minimize the impact of temperature. Piezoelectric ceramic sensor collects the stress wave generated by the actuator. In the data collection process, in order to make the test proceed smoothly, the specific test steps are as follows:

Step 1: according to the test design, the specimen was cut

Step 2: it was found that the surface temperature of GFRP specimens increased significantly, and all specimens were placed on the test bench for 1 hour

Step 3: After the temperature of GFRP specimens was stable, the epoxy resin was applied at the designated position, and the two piezoelectric ceramic sensors were fixed. In this way, there was a layer of epoxy resin between the piezoelectric ceramic sensor and the specimen. If the thickness of each epoxy resin was different, it may affect the collected data. Therefore, when fixing the sensor, the thickness of the epoxy resin layer should be the same as far as possible

Step 4: the instrument was switched on for data collection in quiet environment

Step 5: MATLAB was used to process the collected data

4. Analysis of Test Results

4.1. Time-Domain Signal Diagram Analysis. As shown in Figure 6, the horizontal coordinate represents the data acquisition time is 1 s, and the vertical coordinate represents the voltage value of the collected signal. The data acquisition system collected 2 million data in 1 s. The voltage value of the signal can reflect the damage degree of the specimen to a certain extent. The greater the damage degree of the specimen, the smaller the voltage value. By comparing the voltage values of different specimens, it is concluded that whether the damage change of specimens is consistent with that of actual specimens.

The number of cracks in group A is 1, and the depth of the crack increases gradually from 0 mm to 7 mm. As shown in Figure 6, it can be obviously found that the maximum

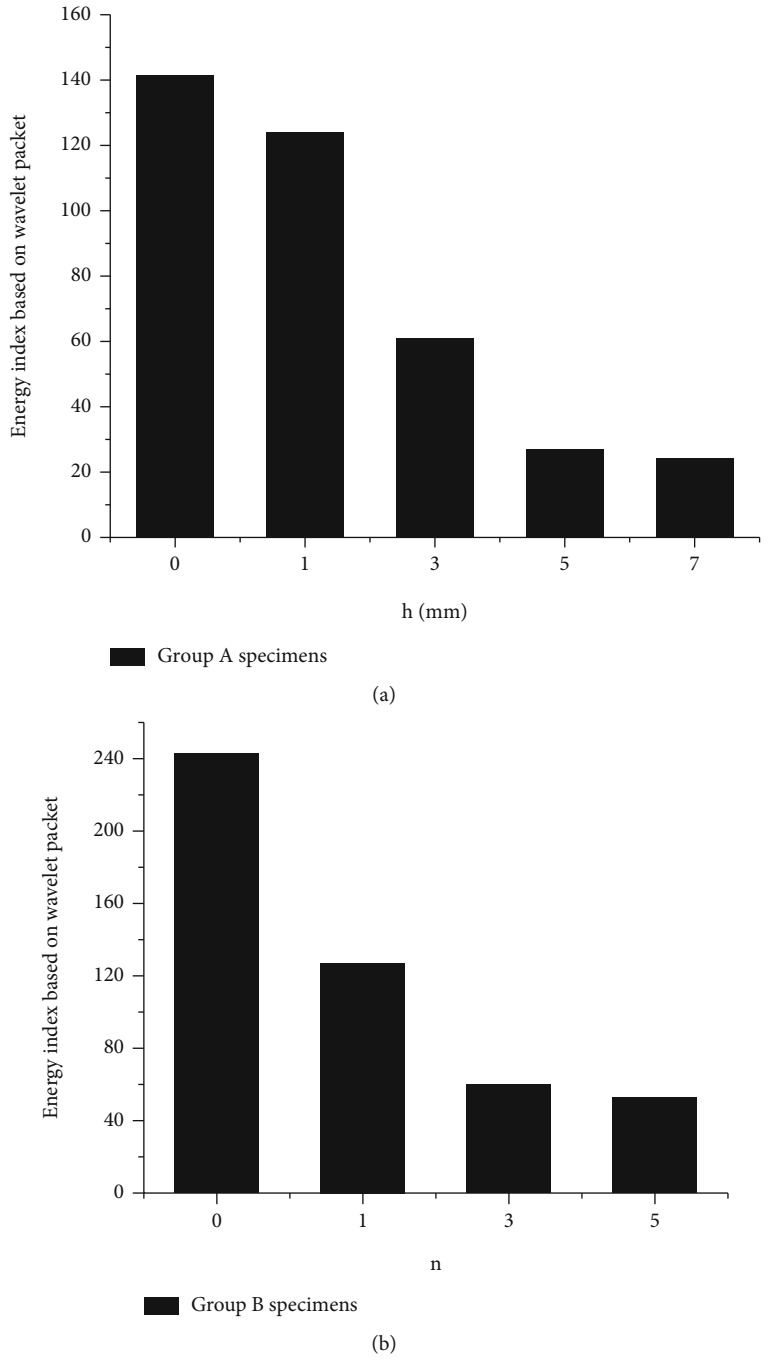

Figure 9: Energy based on wavelet packet. (a) Group A specimens. (b) Group B specimens.

voltage of specimen GP-A-0-0 is 0.00978 V, which is the largest in group A, followed by specimen GP-A-1-1. The smallest voltage value of group A is GP-A-1-7, which is 0.00395 V. It can be concluded that with the increase of crack depth, the voltage value is gradually reduced.

The depth of cracks in group B is 3 mm, and the number of cracks increases gradually from 0 to 5. As shown in Figure 7, it can be obviously found that the maximum voltage value of specimen GP-B-0-0 is the largest in group B, which is 0.013 V, followed by specimen GP-B-1-3. The lowest voltage value of group B is GP-B-5-3, which is 0.0051 V. It can be concluded that with the increase of the number of cracks, the voltage value also decreases gradually.

The specific variation of voltage value of group A and B specimens is shown in Figure 8. In summary, the change of voltage value can reflect the damage change of the specimen to a certain extent, and the smaller the voltage value is, the greater the damage degree is.

4.2. Energy Analysis. As shown in Figure 9, in order to analyze the change of stress wave energy, the energy method based on wavelet packet is used to estimate the energy of

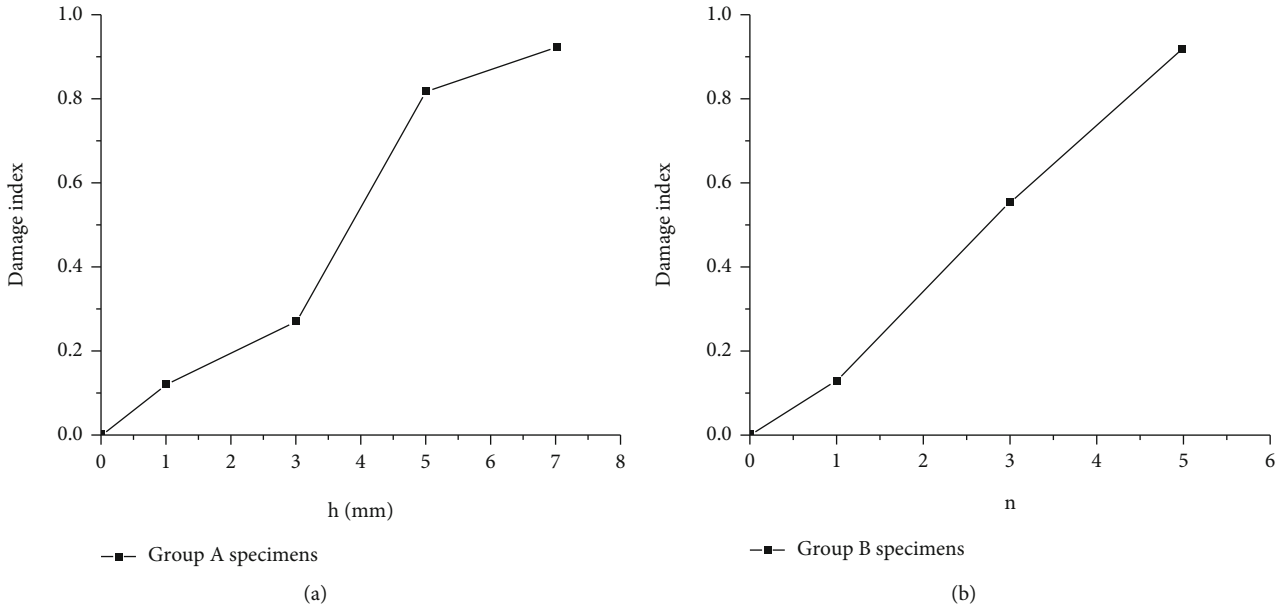

Figure 10: Index based on wavelet packet. (a) Group A specimens. (b) Group B specimens.

the received signal. In group A, the crack depth increases gradually from 0 mm to 7 mm, while the energy index based on wavelet packet decreases gradually from 142.8 to 24.1. With the increasing number of cracks in group B, from 0 crack to 5 cracks, the voltage value gradually decreased from 242.9 to 52.9. The test results showed that the decrease of energy based on wavelet packet can reflect the damage trend of GFRP specimens to a certain extent.

In addition, in terms of the maximum voltage value and the energy based on wavelet packet, the specimen GP-B-0-0 is greater than that of the specimen GP-A-0-0, which is due to the different input parameters on the signal transmitter. The stop frequency of group A is 100 kHz, while that of group B is 500 kHz. Similarly, the difference between specimen GP-A-1-3 and specimen GP-B-1-3 is also the reason.

The time domain signal graph analysis, voltage value analysis, and energy analysis based on wavelet packet can only analyze the damage change of the specimen and cannot judge the specific degree of specimen damage. Therefore, the damage index (DI) based on wavelet packet is introduced, which is presented and discussed in the previous paper. As shown in Figure 10, it is based on the change of wavelet packet damage index. It can be seen from Figure 10(a) that in group A specimens, the corresponding damage indexes of the specimens with crack depth of 0 mm, 1 mm, 3 mm, 5 mm, and 7 mm are 0, 0.11, 0.25, 0.82, and 0.92, respectively, that is, the damage degrees of the specimens are 0, 11%, 25%, 82%, and 92%, respectively. It shows that the deeper the crack depth of the specimen, the greater the damage index and the greater the damage degree. Similarly, as shown in Figure 10(b), group B specimens are analyzed. The more cracks in the specimen, the greater the damage index and the greater the damage degree.

The damage index of the specimens GP-A-1-3 and GP-B-1-3 is different. The possible reasons are as follows: (1) the output frequencies of the signal transmitters of the two are different, resulting in different collected signals. (2) The difference of the sensor itself will have an impact on the collected data. (3) GFRP materials are not homogeneous materials, and their own differences will affect the collected data. Based on the above influencing factors, the wavelet packet damage index can only evaluate specimens in the same group and cannot compare specimens in different groups.

The above experimental results show that the piezoelectric ceramic sensor is expected to be used to detect the damage change of GFRP by the active induction method. However, some shortcomings of the active induction method are also exposed in the test. Although the change trend of structural damage of GFRP can be judged by the change of the maximum voltage value and the energy value based on the wavelet packet, the degree of structural damage and the specific location of damage cannot be specifically identified. Before practical application, it is necessary to consider the distance between the sensor producing stress waves, the sensor receiving stress wave, and the temperature of the working environment. In addition, the types of GFRP and its working environment will also have a great impact on the test data.

5. Conclusions

In this paper, piezoelectric ceramic sensors are used to detect the damage of GFRP, and the collected data are processed by the active induction method based on wavelet packet and the principle of damage index. It is found that as the crack depth changes from 0 to 7 mm, the time domain signal diagram of the group A specimens changes significantly. The voltage value is reduced from 0.00978 V to 0.00395 V, and the energy based on wavelet packet is reduced from 142.8 to 24.1. The damage index based on wavelet packet increases from 0 to 0.92. It can be seen that as the depth of the specimen crack increases, the voltage value decreases, the energy

decreases, and the damage index increases. In the same way, analyzing the group B specimens, it can be obtained that as the number of cracks in the specimens increases, the voltage value decreases, the energy decreases, and the damage index increases. The experimental results show that the maximum voltage value of the specimen, the energy based on wavelet packet and the damage index based on wavelet packet can accurately judge the damage change of the specimen. The active induction method based on piezoelectric ceramic sensors can detect the damage change of GFRP specimens in real time. It provides an effective method for damage analysis of GFRP composite civil materials.

Data Availability

All data that support the findings of this study are available from the corresponding author, upon reasonable request.

Conflicts of Interest

The authors declare that there are no conflicts of interests to this work. We do not have any commercial or associative interest that represents a conflict of interest in connection with the work submitted.

Acknowledgments

This work is financially supported by the National Natural Science Foundation of China (NSFC, 51408057) and the Science and Technology Project of the Ministry of Housing and Urban-Rural Development of China (MOHURD, 2021-k-086).

References

[1] H. Zhou, Y. Liu, Y. Lu et al., "In-situ crack propagation monitoring in mortar embedded with cement-based piezoelectric ceramic sensors," *Construction and Building Materials*, vol. 126, pp. 361–368, 2016.

[2] D. Wang, Q. Wang, H. Wang, and H. Zhu, "Experimental study on damage detection in timber specimens based on an electromechanical impedance technique and RMSD-based mahalanobis distance," *Sensors*, vol. 16, no. 10, p. 1765, 2016.

[3] J. Xu, J. Hao, H. Li, M. Luo, W. Guo, and W. Li, "Experimental damage identification of a model reticulated shell," *Applied Sciences*, vol. 7, no. 4, p. 362, 2017.

[4] Q. Kong, R. H. Robert, P. Silva, and Y. Mo, "Cyclic crack monitoring of a reinforced concrete column under simulated pseudo-dynamic loading using piezoceramic-based smart aggregates," *Applied Sciences*, vol. 6, no. 11, p. 341, 2016.

[5] G. Song, C. Wang, and B. Wang, "Structural health monitoring (SHM) of civil structures," *Applied Sciences*, vol. 7, no. 8, p. 789, 2017.

[6] D. Hughi and H. Marzouk, "Crack width monitoring system for reinforced concrete beams using piezo-ceramic sensors," *Journal of Civil Structural Health Monitoring*, vol. 5, no. 1, pp. 57–66, 2015.

[7] C. A. Perez-Ramirez, A. Y. Jaen-Cuellar, M. Valtierra-Rodriguez et al., "A two-step strategy for system identification of civil structures for structural health monitoring using wavelet transform and genetic algorithms," *Applied Sciences*, vol. 7, no. 2, p. 111, 2017.

[8] S. Yan, H. Ma, P. Li, G. Song, and J. Wu, "Development and application of a structural health monitoring system based on wireless smart aggregates," *Sensors*, vol. 17, no. 7, p. 1641, 2017.

[9] F. Wang, S. C. Ho, L. Huo, and G. Song, "A novel fractal contact-electromechanical impedance model for quantitative monitoring of bolted joint looseness," *Ieee Access*, vol. 6, no. 6, pp. 40212–40220, 2018.

[10] N. Kaur and S. Bhalla, "Combined energy harvesting and structural health monitoring potential of embedded piezo-concrete vibration sensors," *Journal of Energy Engineering*, vol. 141, no. 4, p. D4014001, 2015.

[11] J. Xu, C. Wang, H. Li, C. Zhang, J. Hao, and S. Fan, "Health monitoring of bolted spherical joint connection based on active sensing technique using piezoceramic transducers," *Sensors*, vol. 18, no. 6, p. 1727, 2018.

[12] H. Mei, M. F. Haider, R. Joseph, A. Migot, and V. Giurgiutiu, "Recent advances in piezoelectric wafer active sensors for structural health monitoring applications," *Sensors*, vol. 19, no. 2, p. 383, 2019.

[13] H. N. Li, L. Ren, Z. G. Jia, T. H. Yi, and D. S. Li, "State-of-the-art in structural health monitoring of large and complex civil infrastructures," *Journal of Civil Structural Health Monitoring*, vol. 6, no. 1, pp. 3–16, 2016.

[14] Y. Chen and X. Xue, "Advances in the structural health monitoring of bridges using piezoelectric transducers," *Sensors*, vol. 18, no. 12, p. 4312, 2018.

[15] Y. He, X. Chen, Z. Liu, and Y. Qin, "Piezoelectric self-sensing actuator for active vibration control of motorized spindle based on adaptive signal separation," *Smart Materials and Structures*, vol. 27, no. 6, article 065011, 2018.

[16] D. F. Wang, X. Lou, A. Bao, X. Yang, and J. Zhao, "A temperature compensation methodology for piezoelectric based sensor devices," *Applied Physics Letters*, vol. 111, no. 8, article 083502, 2017.

[17] B. Dong, Y. Liu, L. Qin et al., "In-situ structural health monitoring of a reinforced concrete frame embedded with cement-based piezoelectric smart composites," *Research in Nondestructive Evaluation*, vol. 27, no. 4, pp. 216–229, 2016.

[18] P. Kijanka, A. Manohar, F. Lanza di Scalea, and W. J. Staszewski, "Damage location by ultrasonic lamb waves and piezoelectric rosettes," *Journal of Intelligent Material Systems and Structures*, vol. 26, no. 12, pp. 1477–1490, 2015.

[19] S. Zhang, Y. Zhang, and Z. Li, "Ultrasonic monitoring of setting and hardening of slag blended cement under different curing temperatures by using embedded piezoelectric transducers," *Construction and Building Materials*, vol. 159, pp. 553–560, 2018.

[20] H. H. Pan and M. W. Huang, "Piezoelectric cement sensor-based electromechanical impedance technique for the strength monitoring of cement mortar," *Construction and Building Materials*, vol. 254, article 119307, 2020.

[21] H. H. Pan, C. K. Wang, and Y. C. Cheng, "Curing time and heating conditions for piezoelectric properties of cement-based composites containing PZT," *Construction and Building Materials*, vol. 129, pp. 140–147, 2016.

[22] P. Pillatsch, B. L. Xiao, N. Shashoua, H. M. Gramling, E. M. Yeatman, and P. K. Wright, "Degradation of bimorph piezoelectric bending beams in energy harvesting applications," *Smart Materials and Structures*, vol. 26, no. 3, article 035046, 2017.

[23] R. Caliò, U. B. Rongala, D. Camboni et al., "Piezoelectric energy harvesting solutions," *Sensors*, vol. 14, no. 3, pp. 4755–4790, 2014.

[24] Y. Zheng, D. Chen, L. Zhou, L. Huo, H. Ma, and G. Song, "Evaluation of the effect of fly ash on hydration characterization in self-compacting concrete (SCC) at very early ages using piezoceramic transducers," *Sensors*, vol. 18, no. 8, p. 2489, 2018.

[25] Q. Kong, S. Fan, X. Bai, Y. L. Mo, and G. Song, "A novel embeddable spherical smart aggregate for structural health monitoring: part I. fabrication and electrical characterization," *Smart Materials and Structures*, vol. 26, no. 9, article 095050, 2017.

[26] D. Wang, H. Song, and H. Zhu, "Embedded 3D electromechanical impedance model for strength monitoring of concrete using a PZT transducer," *Smart Materials and Structures*, vol. 23, no. 11, article 115019, 2014.

[27] Y. S. Roh, *Built-in Diagnostics for Identifying an Anomaly in Plates Using Wave Scattering*, Stanford University, 1999.

[28] G. Du and Q. Kong, "An experimental feasibility study of pipeline corrosion pit detection using a piezoceramic time reversal mirror," *Smart Materials and Structures*, vol. 25, no. 3, article 037002, 2016.

[29] G. Du and Q. Kong, "Multiple cracks detection in pipeline using damage index matrix based on piezoceramic transducer-enabled stress wave propagation," *Sensors*, vol. 17, no. 8, p. 1812, 2017.

[30] Q. Feng, Q. Kong, and G. Song, "Damage detection of concrete piles subject to typical damage types based on stress wave measurement using embedded smart aggregates transducers," *Measurement*, vol. 88, pp. 345–352, 2016.

[31] J. Zhang, Y. Huang, and Y. Zheng, "A feasibility study on timber damage detection using piezoceramic-transducer-enabled active sensing," *Sensors*, vol. 18, no. 5, p. 1563, 2018.

[32] L. Huo, F. Wang, H. Li, and G. Song, "A fractal contact theory based model for bolted connection looseness monitoring using piezoceramic transducers," *Smart Materials and Structures*, vol. 26, no. 10, article 104010, 2017.

[33] F. Wang and L. Huo, "A piezoelectric active sensing method for quantitative monitoring of bolt loosening using energy dissipation caused by tangential damping based on the fractal contact theory," *Smart Materials and Structures*, vol. 27, article 015023, 2018.

[34] H. Yin, T. Wang, D. Yang, S. Liu, J. Shao, and Y. Li, "A smart washer for bolt looseness monitoring based on piezoelectric active sensing method," *Applied Sciences*, vol. 6, no. 11, p. 320, 2016.

[35] G. Song, W. Li, B. Wang, and S. Ho, "A review of rock bolt monitoring using smart sensors," *Sensors*, vol. 17, no. 4, p. 776, 2017.

[36] D. Xu, S. Banerjee, Y. Wang, S. Huang, and X. Cheng, "Temperature and loading effects of embedded smart piezoelectric sensor for health monitoring of concrete structures," *Construction and Building Materials*, vol. 76, pp. 187–193, 2015.

[37] Q. Feng and H. Xiao, "Damage detection of concrete piles subject to typical damages using piezoceramic based passive sensing approach," *Journal of Vibroengineering*, vol. 18, pp. 801–812, 2016.

[38] P. Liu, Y. Hu, B. Geng, and D. Xu, "Investigation on novel embedded piezoelectric ultrasonic transducers for corrosion monitoring of reinforced concrete," *Smart Materials and Structures*, vol. 28, no. 11, article 115041, 2019.

[39] Q. Kong, H. Chen, Y. L. Mo, and G. Song, "Real-time monitoring of water content in sandy soil using shear mode piezoceramic transducers and active sensing—a feasibility study," *Sensors*, vol. 17, no. 10, p. 2395, 2017.

[40] Q. Kong, R. Wang, G. Song, Z. ". J.". Yang, and B. Still, "Monitoring the soil freeze-thaw process using piezoceramic-based smart aggregate," *Journal of Cold Regions Engineering*, vol. 28, no. 2, p. 06014001, 2014.

[41] J. Rao, M. Ratassepp, D. Lisevych, M. Hamzah Caffoor, and Z. Fan, "On-line corrosion monitoring of plate structures based on guided wave tomography using piezoelectric sensors," *Sensors*, vol. 17, no. 12, p. 2882, 2017.

[42] F. Qin, Q. Kong, M. Li, Y. L. Mo, G. Song, and F. Fan, "Bond slip detection of steel plate and concrete beams using smart aggregates," *Smart Materials and Structures*, vol. 24, no. 11, article 115039, 2015.

[43] S. Li and G. Xiao, "On lateral compression of circular aluminum, CFRP and GFRP tubes," *Composite Structures*, vol. 232, article 111534, 2020.